Beam formation and transport in the BATMAN Upgrade test facility

Niek den Harder,[a] Federica Bonomo, Andrew Hurlbatt, Riccardo Nocentini, Christian Hopf, Ursel Fantz, and the NNBI Team
Max-Planck-Institut für Plasmaphysik, Garching bei München, Germany

(Dated: 24 January 2020)

In the BATMAN Upgrade test facility, an RF-driven negative hydrogen ion source is developed in support of the ITER NBI. Its 5 × 14 apertures represent approximately one ITER beamlet group. Diagnostics include a tungsten wire calorimeter, a copper calorimeter, and two arrays of beam emission spectroscopy lines of sight.

When the RF-power is increased at fixed extraction potential, the extracted current density saturates. This is due to scraping of the beamlet by the extraction grid; a method is developed to characterize the injected current density. This current density can vary locally, e.g. due to the E×B drift induced by the filter field. A procedure is introduced to infer the vertical injected current density profile from the behaviour of the different beam emission spectroscopy lines of sight during an RF-power scan.

The injected current density profile is used to calculate aperture specific beamlet properties with IBSimu. The beamlet properties are projected towards the calorimeters with the ABC3D code, and compared with measurements to benchmark the current density profile and IBSimu calculations. Beamlet-to-beamlet variations of power and width in the tungsten wire calorimeter are well reproduced. It is crucial to include heat transfer in the copper calorimeter to reproduce the measured profiles.

I. INTRODUCTION

Neutral Beam Injection (NBI) will be the main heating system of ITER, with 33 MW delivered to the plasma by 2 injectors that accelerate deuterium to 1 MeV through 1280 apertures each[1]. The ITER NBI system is based on negative ions since the neutralization efficiency of positive ion beams is vanishingly small at energies above 100 keV/amu. Negative hydrogen ion NBI systems are challenging since it is difficult to extract a large ion current homogeneously while keeping the coextracted electron current sufficiently low.

The BATMAN Upgrade (BUG) test facility represents approximately one ITER beamlet group with its 70 apertures, but has a total high-voltage capacity of only 45 kV[2]. It aims to optimize the extracted current density from protium and deuterium plasmas, while operating at low filling pressure (0.3 Pa) with coextracted electron-to-ion ratios smaller than one. Due to stripping losses in the ITER acceleration grids, it is necessary to demonstrate extracted current densities of 329 A/m^2 in protium, and 286 A/m^2 in deuterium[3,4]. In addition, there are ITER requirements on the pulse length (3600 s in D), homogeneity (± 10%), and divergence[1].

An increase in divergence leads to larger power loads inside the beamline, leaving less power available to heat the plasma. The ITER beamlines are designed assuming a double Gaussian profile for the angular distribution of the beamlets with a core carrying 85 % of the power at a divergence in the range 3-7 mrad, and a halo at a divergence of 15 mrad[1] or 30 mrad[5]. Based on modeling, the expected divergence is easily reached in the ITER heating neutral beam. In BUG the minimum divergence is expected to be in the range 11-14 mrad because the grid system is optimized for high current extraction at 45 kV total voltage.

The divergence is a function of the current density, thus aperture-to-aperture variations lead to suboptimal ion optics. The current density can be vertically inhomogeneous in BUG due to the E×B drift caused by the magnetic filter field. This paper presents a method to infer the vertical current density profile from the behaviour of the different beam emission spectroscopy lines of sight during RF power scans.

The vertical current density profile is used as input to make beamlet specific ion optics calculations with the IBSimu code. The beamlets are projected towards the Tungsten Wire Calorimeter (TWC) and copper calorimeter with the ABC3D code to benchmark the current density profile and IBSimu calculations[6]

II. COMPUTATIONAL METHODS

Ion optics calculations were performed with IBSimu, a computer simulation package for ion optics, plasma extraction and space charge dominated ion beam transport using Vlasov iteration[7,8]. Protium ions enter the simulation box 2 mm before the plasma grid with a starting energy of 3 eV, and a parallel and perpendicular temperature of 1 eV. The injected current density, i.e. the current density at the injection plane, is varied in the simulations, the other input parameters are kept constant.

Coextracted electrons are neglected, since they contribute $\sqrt{m_H/m_e} \approx 43$ times less to the space charge at identical current density. The ion to electron ratio was below 1 for all shown results. The background gas density profile and associated stripping losses are not included in the simulations, since it has negligible influence on the space charge.

[a] Electronic mail: niek.den.harder@ipp.mpg.de

It is assumed that 10 mm after the grounded grid, space charge compensation has set in, and there is no net local charge density and associated electric field that changes the angular distribution of the beamlet[9]. The particles which exit the grounded grid are used to define an extracted current density, which can be smaller than the injected current density when beam particles hit the grids. The simulated angular distribution is analyzed in two ways. A single Gaussian divergence is determined, a standard evaluation procedure. In addition, a double Gaussian is fit to the distribution: a core Gaussian with a smaller divergence, and a halo Gaussian with a larger divergence. Adding the two components geometrically recovers the single Gaussian divergence.

Power densities are calculated with the ABC3D code by extrapolating the beamlets after the grid system[6]. The positions, directions, initial sizes, and divergences of the double Gaussian power density distribution, are taken from the IBSimu calculations. The divergence $\theta_{1/e}$ is half the opening angle of a cone with power densities that are $1/e$ of the on-axis power density. The normalized power density for one single divergence beamlet as function of parallel ($l_\parallel$) and perpendicular ($l_\perp$) distance with respect to the beamlet axis is given by

$$F\left(l_\parallel, l_\perp\right) = \frac{1}{2\pi\sigma_{l_\perp}^2} \exp\left(-\frac{l_\perp^2}{2\sigma_{l_\perp}^2}\right) \tag{1}$$

with

$$\sigma_{l_\perp} = \frac{l_\parallel \tan\left(\theta_{1/e}\right)}{\sqrt{2}} + \sigma_0. \tag{2}$$

where σ_0 is the initial size of the beamlet.

In order to include transport effects such as deflection after the grid system, and correctly describe the interaction of the beam with spectroscopic diagnostics, a different modeling approach is needed. BBCNI is such a code, which tracks particles through electric and magnetic fields[10]. This approach is more CPU intensive, output data from a single BBCNI run will be shown to assess the validity of the double Gaussian fit and the impact of transport effects.

Heat transport in the copper calorimeter was modeled with finite element methods in Ansys, taking into account the inertial cooling.

III. EXPERIMENTAL LAYOUT

In BUG, negative hydrogen ions are extracted from an RF created plasma[11]. The source consists of three regions: the driver region where the 1 MHz RF is coupled to the plasma, the expansion region where the plasma expands into the source vessel, and the extraction region. A magnetic filter field separates the expansion region from the extraction region. The source is caesiated to improve the negative hydrogen ion yield via an increase of the surface production rate[12].

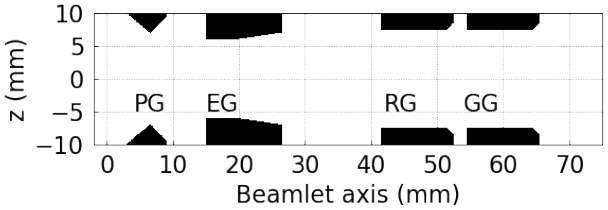

FIG. 1: A schematic view of a BUG single aperture.

The 14 mm ⌀ apertures are arranged in a rectangular beamlet group of 5 × 14 apertures with 20 mm distance between apertures. The extraction system consists of 4 grids: the plasma grid (PG), the extraction grid (EG), the repeller grid (RG), and the grounded grid (GG), as shown in Figure 1. Between the PG and EG, the extraction potential is applied, which ranges from 2 to 10 kV. Between the EG and GG there is an acceleration potential. The RG can be biased up to 2 kV to prevent back-acceleration of positive ions. The total high-voltage is limited to 45 kV. The extracted current is measured as the current which passes the extraction grid. This is a good proxy to compare with the simulations, since losses at the RG and GG are minimal for the shown discharges.

A vertical current through the plasma grid up to 3 kA creates a filter field with a strength on the order of a few mT in the extraction region. The field magnetizes the electrons but not the ions, and reduces both the electron temperature and density in front of the plasma grid[13]. This improves the extracted ion to electron ratio by suppressing negative ion destruction and reducing the amount of electrons that are available to extract. As a drawback, it induces an E×B drift that causes a vertical asymmetry in electron density in front of the PG[14,15].

To prevent acceleration of the coextracted electrons, permanent magnets deflect them onto the EG, alternatingly to the left and right for different aperture rows. The beam ions exit the grid system with a deflection angle on the order of a degree due to their larger mass.

BUG is equipped with two Beam Emission Spectroscopy (BES) viewing arrays, with a vertical array of horizontal observation chords at 26 cm (BES1) and 129 cm (BES2) from the grounded grid[2]. The Doppler shifted beam emission is fitted to determine a divergence. Since the BES measures several beamlets at once, the signal contains additional broadening mechanisms, such as for example the left-right deflection of the beamlets. The spectroscopic divergences are therefore not directly comparable to modeled single beamlet divergences. A forward model of beam formation, transport, and interaction with the optical system is needed to correctly take into account the different effects contributing to the spectra. The code BBCNI is especially developed for this purpose[10].

BUG has a tungsten wire calorimeter, which is placed 19 cm from the grounded grid and diagnoses the central column of beamlets with 11 wires[16]. The measured power

density profile is fitted with a 14 2D Gaussians, with independent amplitudes, positions, and widths. Horizontally neighbouring beamlets are included in the fit, but have the same fit parameters as the central Gaussian. BUG was operated with reduced parameters at the beginning of the campaign, when increasing the performance the tungsten wires melted at a local power density of 12 MW/m^2[16].

The beam is dumped on a copper calorimeter 2.2 meters away from the grounded grid[2]. The horizontal and vertical profile are measured by 29 thermocouples inside 4 cm large squares, which are milled into a 10 mm copper plate separated by 5 mm deep slits. This leads to a significant amount of heat conduction between the squares. An improved long-pulse calorimeter is foreseen[17].

IV. RESULTS

A. Measurement interpretation: injected current density

In the experiments, the extracted current is measured as a sum over all the apertures. In the simulations, the injected current density for a single aperture is needed as input. To bridge this gap, the injected current is deduced from the extracted current measurements during an RF power scan. A current density profile is inferred from the differences between the vertical BES lines of sight.

RF power scans were performed at reduced parameters to have the TWC available as diagnostic. The extraction and acceleration potentials were fixed at their optimum ratio, and protium was used at 0.4 Pa filling pressure. Figure 2 shows the measured extracted current density for two scans at different U_{ext}. Initially the current density increases linearly with the RF power, but at higher RF power the extracted current saturates and the EG current increases strongly[18]. The same effect is present in the ion optics simulations at increasing injected current density, but the effect starts at extracted current densities that are approximately 20% higher. In the simulations the extracted current saturates due to scraping of the beamlets on the extraction grid. Since the behaviours match, the RF power is interpreted as an injected current density. The proportionality is obtained by fitting the linear part of the extracted current density for each RF power scan. This enables a direct comparison between measurements and calculations, and allows to distinguish discharges with the same extracted current.

The injected current density is a summed over all the apertures, to correctly model BUG the spatial profile of the current density should be taken into account as well. To demonstrate a method to determine the current density profile, the RF power scan at a (U_{ext}, U_{acc}) of (5,25) kV shown in Figure 2 was performed with a plasma grid current of 2.5 kA. This generates a large vertical inhomogeneity due to the large E×B drift, which results in different BES divergences for the vertical measurement

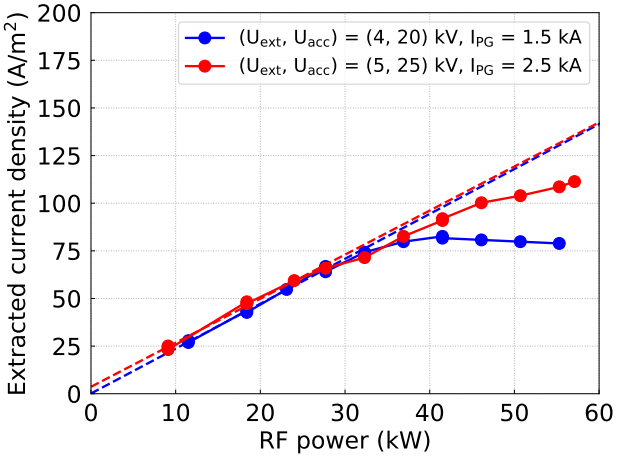

FIG. 2: The measured extracted current saturates when the RF power increases. The dashed lines are fit to the linear part of the measurements.

positions, as shown in Figure 3. Only three of the five lines of sight are plotted for clarity. Because the scan is at reduced parameters, the expected minimum single beamlet divergence is approximately 18 mrad. The BES divergences are much higher because of the left-right deflection and the contribution of high-divergence beamlets as result of the inhomogeneity. At identical injected current density the ion optics should be the same, so the different measurements should fall on a common curve. Shifting the different lines of sight to obtain one curve is thus a way to determine the vertical profile of the injected current density. The sum of shifts is restricted to 0. This approach assumes that the absolute inhomogeneity does not change with the RF power. The shifted curves overlap well, which is an indication that this is a reasonable assumption for this scan.

Figure 4 shows the fitted offsets for BES1 and BES2. The general trends agree well, but due to beamlet mixing the inhomogeneity measured by BES2 is less pronounced. The BES1 offsets are used to calculate the vertical injected current density profile of the measured discharges by adding the interpolated offsets to the average current density. Horizontally the injected current density is assumed to be constant. The aperture-specific injected current density is used as input for single aperture IBSimu calculations, thus allowing correct beam modeling even for inhomogeneous discharges.

B. Modeling benchmark: calculating diagnostics

The last section presented measurement analysis to derive a local injected current density profile. This section uses those profiles as input for modeling to calculate the calorimetric diagnostics. There are two main research objectives. Firstly to assess if the BES-shift derived cur-

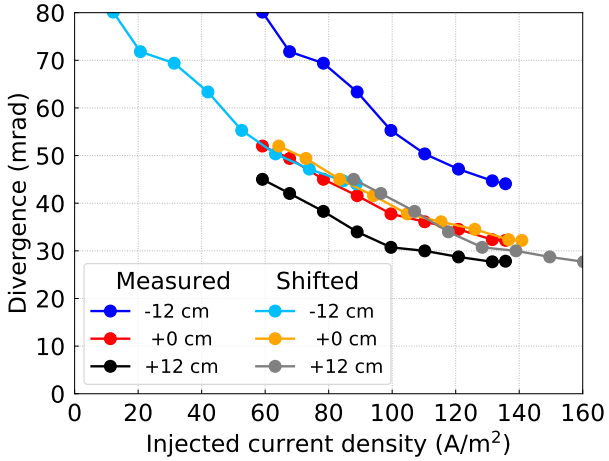

FIG. 3: Different BES 1 vertical positions measure a different divergence during the P_{RF} scan at a (U_{ext}, U_{acc}) of (5,25) kV.

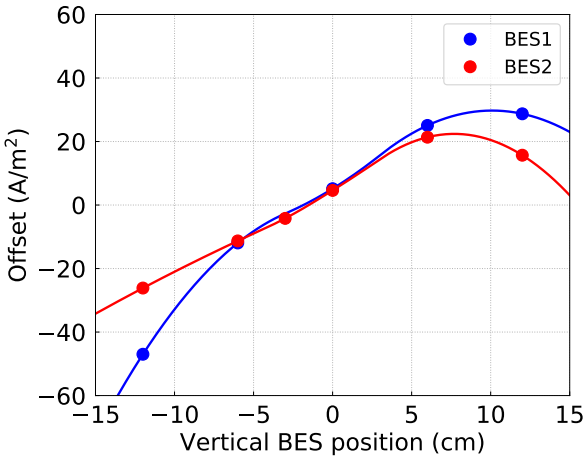

FIG. 4: The injected current density inhomogeneity for the P_{RF} scan at a (U_{ext}, U_{acc}) of (5,25) kV.

rent density matches direct measurements. Secondly to test if the modeled divergences, which are significantly lower than the BES measurements, are compatible with the measured power density profiles. After a brief description of the method, and some general observations, these two research objectives will be described in detail.

IBSimu simulations were performed for the extraction and acceleration potentials of the measurements, at several current densities. The simulations were done for the horizontally central aperture that is vertically just below the middle of the grid. The magnetic field differs only slightly between the different apertures, simulating a single aperture saves a factor of 70. To include the left-right deflection due to the alternating direction of the deflection magnets, the horizontal position and direction is flipped for the different aperture rows.

A double Gaussian represents the simulated angular distribution much better than a single Gaussian, especially at low current densities where the increase in overall divergence is mostly due to an increase of the more divergent halo fraction. At high current densities, the angular distribution departs from a Gaussian, and the fit quality decreases. This is especially the case for the horizontal angular distribution, which becomes asymmetric when the edge of the beamlet is scraped by the extraction grid when it comes too close under the influence of the deflection field. The simulated beamlet sizes, positions, directions, and angular distributions are used to project the beamlets towards the diagnostics.

Figure 5 shows the scaled TWC power density for BUG discharge #117493, which had a (U_{ext}, U_{acc}) of (5,25) kV, and an average injected current density of 136 A/m^2. For the vertical current density profile, the BES1 offsets shown in Figure 4 are added to 136 A/m^2, so that the minimum current density at the bottom is 81 A/m^2, 55 A/m^2 lower. The maximum current density at the top is 165 A/m^2, 29 A/m^2 higher, which is in the saturated regime where particles are lost on the extraction grid as shown in Figure 2. Due to the small number of intensity levels of the IR camera, the measured data shows steps when the intensity is low. The white line indicates a broken tungsten wire. Calculated data in the form of extrapolated Gaussians and a full BBCNI particle tracking simulation are shown as well. The BBCNI data is still under analysis, it is shown to illustrate the impact of modeling the full distribution instead of using a double Gaussian fit. There is a reasonable agreement between measured and calculated data. The beamlet deflection seems to be overestimated by the ABC3D calculation, and matches better in the BBCNI profile. The ABC3D data and BBCNI data agree well in the lower half of the grid. At higher current densities, as is the case in the upper half of the grid, particles are lost on the extraction grid. Because this happens on one side when the beamlet is deflected in the grid system, the distribution becomes asymmetric and is thus no longer well characterized by a double Gaussian. Because of the zig-zag positioning as result of beamlet deflection, the beamlets are closer to each other horizontally, and partly overlap. This effect is taken into account in the TWC analysis.

The calculated beamlet-to-beamlet variations are a consequence of the injected current density profile, which is determined with the relatively indirect BES-shift procedure. To assess how well this procedure performs, Figure 6 shows the measured TWC integral, and calculated power per beamlet. The measured profile is normalized to the calculated power. The calculated beamlet power does not exactly follow the injected current density profile shown in Figure 4 due to scraping. The measured power per beamlet generally agrees well with the profile estimated with the BES-shift, even though that procedure is quite indirect. Local variations in the profile are averaged out and cannot be resolved with the BES-shift

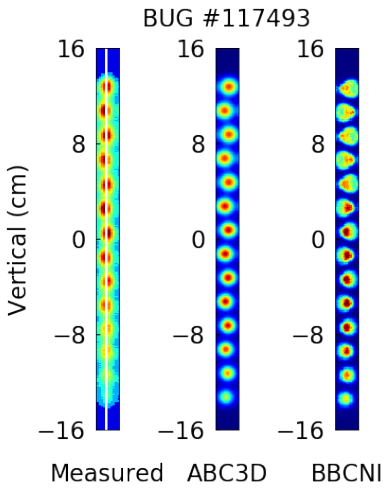

FIG. 5: The scaled TWC power density for BUG discharge #117493 is shown together with Gaussian extrapolation and BBCNI calculated data.

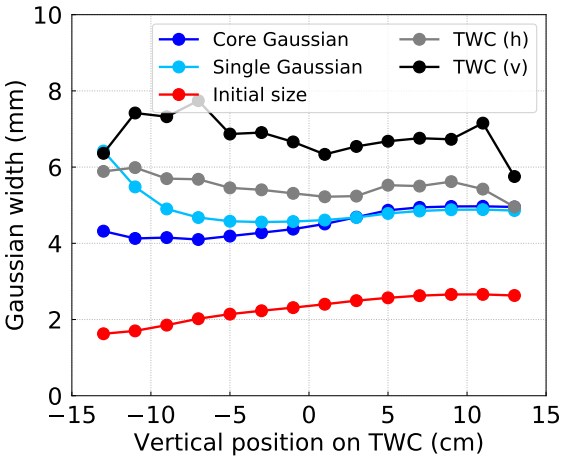

FIG. 7: The calculated widths of the beamlets is compared with the measured TWC widths for BUG discharge #117493.

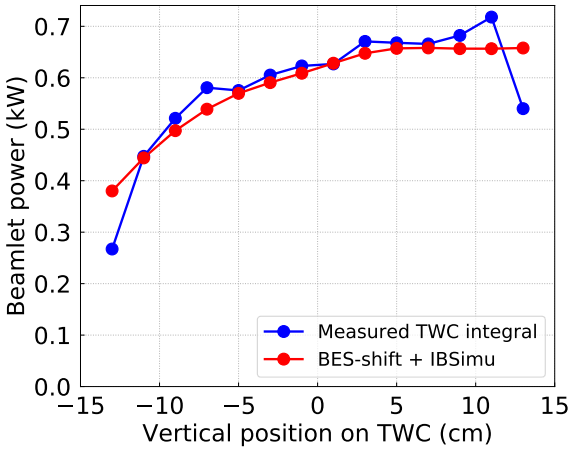

FIG. 6: The TWC measured power per beamlet is compared to the power as determined from the BES-shift and IBSimu calculations for a discharge with 13.6 mA/cm^2 and a (U_{ext}, U_{acc}) of (5,25) kV.

procedure, which only includes 5 lines of sight separated by 6 cm for BES1. Since the TWC is not available for high-performance discharges, it is useful to have an alternative procedure to determine the current density profile, even if it needs a number of discharges.

The width of the beamlet at the TWC is an important benchmark for the IBSimu calculations, because a good agreement would confirm the modeled divergences, which are significantly smaller than the BES divergences. The measured TWC profiles are more peaked than the single Gaussian fit. This leads to an overestimation of the measured width, and is subject of ongoing investigation. The calculated single beamlet width at the TWC is determined with Equation 2. The initial size is a few millimeters, a significant fraction of the final width, and therefore essential to include. The width of the core component of the angular distribution, as well as the width of a single Gaussian interpretation are shown in Figure 7. The width of the core component of the double Gaussian stays relatively constant, indicating that the size increase in the single Gaussian interpretation is due to the halo. Especially at low current densities, the double Gaussian approach is essential to calculate the proper beamlet width. The measured TWC width is shown as well. The vertical width is larger than the horizontal width, which could be due to heat conduction along the wires. The simulated widths are slightly smaller than the measured horizontal widths. It is unclear if this is due to an overestimation of the measured width in the fitting of the measurements, or an underprediction of the initial width or the divergence in the simulations. Generally there is a decent agreement between the measured horizontal width and the IBSimu calculations.

The impact of the initial beamlet size is negligible at the copper calorimeter, which is 2.2 meters downstream from the grounded grids where the beamlets have merged. Because of heat transfer between the calorimeter squares, the measured profiles cannot be directly compared with calculated power density profiles. To account for the heat transfer, calculated power density profiles served as input for FEM modeling. Transient thermal simulations were performed for a 5 second beam onto the copper calorimeter. Figure 8 shows the calculated power density (Calc.), the scaled temperature profiles after heat transfer (FEM), and the measured profiles (Meas.). Including thermal conduction is essential for an accurate description of the measured profile. Although there is a satisfactory match, the synthetic profile generally slightly underpredicts the width, even when thermal transfer ef-

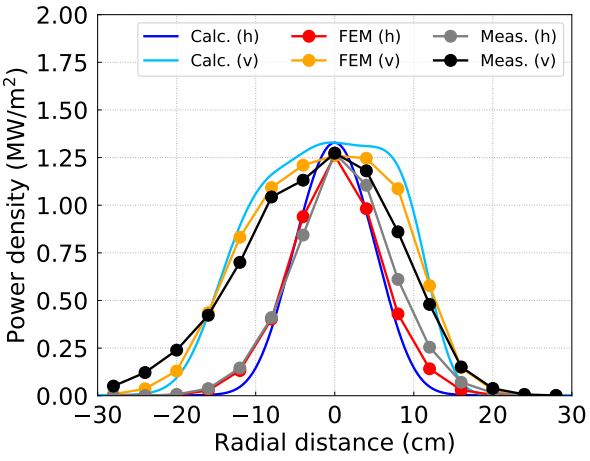

FIG. 8: For BUG discharge #117493, the power density on the copper calorimeter was calculated (Calc.). The calculated profiles served as input for heat transfer calculations that result in temperature profiles (FEM). The measured temperature profiles (Meas.) are shown as well.

fects are included. This is general for all the scans, and consistent with the underprediction of the tungsten wire calorimeter width.

V. CONCLUSIONS

Beam formation and transport was studied in the BUG test facility. A procedure was developed to bridge the gap between experiment, in which the extracted current is measured, and simulation, where the injected current is an input value. In this approach, a proportionality between RF power and extracted current is determined, which enables simulations of discharges with similar extracted current density but different RF power.

A straightforward method to infer the injected current density profile from the vertical profile of the BES divergences has been developed. Beamlet-to-beamlet power profiles determined with this method generally match well with the tungsten wire calorimetry. This method provides a starting point for the injected current density profiles that can be used in further whole-beam modeling.

IBSimu single aperture simulations were benchmarked by comparison of the calculated and measured widths on the TWC and copper calorimeter. The measured TWC horizontal widths are slightly larger than the calculated widths. This might be due to deviations from a single Gaussian in the measured profile, and is subject of ongoing investigation. The width of the beam on the downstream copper calorimeter was analyzed. Heat transfer in the calorimeter was found to play a significant role. When this effect was taken into account, a satisfactory match between measurement and calculation was found. Good general agreement between calculations and different diagnostics inspires confidence in the single aperture calculations, and shows that the beam behaviour can be described with divergences that are significantly lower than the divergence determined with the BES.

[1] INTERNATIONAL ATOMIC ENERGY AGENCY, *ITER Technical Basis*, ITER EDA Documentation Series No. 24 (INTERNATIONAL ATOMIC ENERGY AGENCY, Vienna, 2002).
[2] U. Fantz, F. Bonomo, M. Fröschle, B. Heinemann, A. Hurlbatt, W. Kraus, L. Schiesko, R. Nocentini, R. Riedl, and C. Wimmer, Fusion Engineering and Design (2018), 10.1016/j.fusengdes.2018.12.020.
[3] R. Hemsworth, H. Decamps, J. Graceffa, B. Schunke, M. Tanaka, M. Dremel, A. Tanga, H. D. Esch, F. Geli, J. Milnes, T. Inoue, D. Marcuzzi, P. Sonato, and P. Zaccaria, Nuclear Fusion **49**, 045006 (2009).
[4] A. Krylov and R. Hemsworth, Fusion Engineering and Design **81**, 2239 (2006).
[5] R. S. Hemsworth, D. Boilson, P. Blatchford, M. D. Palma, G. Chitarin, H. P. L. de Esch, F. Geli, M. Dremel, J. Graceffa, D. Marcuzzi, G. Serianni, D. Shah, M. Singh, M. Urbani, and P. Zaccaria, New Journal of Physics **19**, 025005 (2017).
[6] N. den Harder, D. Rittich, G. Orozco, and C. Hopf, Plasma Physics and Controlled Fusion (Submitted).
[7] T. Kalvas, O. Tarvainen, T. Ropponen, O. Steczkiewicz, J. Ärje, and H. Clark, Review of Scientific Instruments **81**, 02B703 (2010), https://doi.org/10.1063/1.3258608.
[8] T. Kalvas, *Development and use of computational tools for modelling negative hydrogen ion source extraction systems*, Ph.D. thesis, University of Jyväskylä (2013).
[9] C. Valerio-Lizarraga, I. Leon-Monzon, and R. Scrivens, Phys. Rev. ST Accel. Beams **18**, 080101 (2015).
[10] A. Hurlbatt, N. den Harder, D. Wünderlich, and U. Fantz, Plasma Physics and Controlled Fusion **61**, 105012 (2019).
[11] B. Heinemann, M. Fröschle, H.-D. Falter, U. Fantz, P. Franzen, W. Kraus, R. Nocentini, R. Riedl, and B. Ruf, AIP Conference Proceedings **1655**, 060003 (2015), https://aip.scitation.org/doi/pdf/10.1063/1.4916472.
[12] L. Schiesko, P. McNeely, U. Fantz, P. Franzen, and the NNBI Team, Plasma Physics and Controlled Fusion **53**, 085029 (2011).
[13] S. Lishev, A. Shivarova, and K. H. Tarnev, Journal of Physics: Conference Series **223**, 012003 (2010).
[14] P. Franzen, L. Schiesko, M. Fröschle, D. Wünderlich, U. Fantz, and the NNBI Team, Plasma Physics and Controlled Fusion **53**, 115006 (2011).
[15] G. J. M. Hagelaar and N. Oudini, Plasma Physics and Controlled Fusion **53**, 124032 (2011).
[16] R. Nocentini, F. Bonomo, U. Fantz, M. Fröschle, B. Heinemann, I. Mario, R. Riedl, and L. Schiesko, Fusion Engineering and Design (2019), 10.1016/j.fusengdes.2018.12.085.
[17] W. Kraus, L. Schiesko, F. Bonomo, U. Fantz, B. Heinemann, and A. Hurlbatt, AIP Conference Proceedings **2052**, 040004 (2018), https://aip.scitation.org/doi/pdf/10.1063/1.5083738.
[18] C. Wimmer, R. Bonomo, A. Hurlbatt, L. Schiesko, U. Fantz, N. den Harder, B. Heinemann, A. Mimo, G. Orozco, M. Agostini, M. Barbisan, M. Brombin, R. Delogu, A. Pimazzoni, C. Poggi, G. Serianni, M. Ugoletti, and P. Veltri, Review of Scientific Instruments **91**, 013509 (2020), https://doi.org/10.1063/1.5129336.